TABLE I
CAPACITANCE OF MICROSTRIP CIRCULAR DISK

ϵ_r=1.0

	1	2	3	4	5	6
d/a	one term approx	10 terms approx	another expression K=1/2	NM	SNA	ALB
0.01	1.0362	1.0421				
0.02	1.0651	1.0778				
0.03	1.0916	1.1110				
0.04	1.1168	1.1426				
0.05	1.1411	1.1730	1.1756			
0.06	1.1647	1.2026	1.2052			
0.07	1.1878	1.2315	1.2342			
0.08	1.2106	1.2599	1.2626			
0.09	1.2330	1.2877	1.2905			
0.1	1.2552	1.3115	1.3180	1.317	1.32	1.20
0.2	1.4702	1.5769	1.5800	1.580	1.57	1.32
0.3	1.6814	1.8265	1.8300	1.830	1.82	1.40
0.4	1.8935	2.0714	2.0751	2.0751	2.06	1.46
0.5	2.1075	2.3142	2.3183	2.3183	2.32	1.50
0.6	2.3239	2.5565	2.5608	2.5607	2.59	1.53
0.7	2.5425	2.7988	2.8034	2.8034	2.88	1.55
0.8	2.7631	3.0415	3.0464	3.0464	3.16	1.57
0.9	2.9855	3.2850	3.2901	3.2901	3.48	1.57
1.0	3.2095	3.5292	3.5346	3.5346	3.81	1.56

ϵ_r=2.65

	1	2	3	4	5	6
d/a	one term approx	10 terms approx	another expression K=1/2	NM	SNA	ALB
0.01	1.0179	1.0210				
0.02	1.0328	1.0404				
0.03	1.0468	1.0590				
0.04	1.0602	1.0769				
0.05	1.0734	1.0945	1.0969			
0.06	1.0862	1.1117	1.1142			
0.07	1.0989	1.1286	1.1311			
0.08	1.1114	1.1454	1.1479			
0.09	1.1239	1.1620	1.1645			
0.1	1.1362	1.1784	1.1809	1.180	1.18	1.14
0.2	1.2588	1.3380	1.3408	1.341	1.33	1.25
0.3	1.3836	1.4943	1.4973	1.497	1.48	1.35
0.4	1.5127	1.6502	1.6533	1.6533	1.64	1.43
0.5	1.6463	1.8066	1.8100	1.8100	1.80	1.51
0.6	1.7839	1.9642	1.9678	1.9678	1.97	1.59
0.7	1.9251	2.1232	2.1269	2.1269	2.15	1.66
0.8	2.0692	2.2835	2.2873	2.2873	2.33	1.73
0.9	2.2158	2.4451	2.4491	2.4491	2.52	1.80
1.0	2.3644	2.6081	2.6122	2.6122	2.72	1.86

tions or using Kobayashi potentials. The solutions for the integrals consist of two expressions in which one is valid for large separation and another for small separation. Using the series expressions derived here, the potential problem of circular parallel capacitor can be readily calculated. The integrals which occur in the study for line capacitance of parallel strip lines [7] can be performed using the present method and the result will be published in a forthcoming paper.

REFERENCES

[1] S. R. Borkar and R. F. H. Yang, "Capacitance of a circular disk for application in microwave integrated circuits," *IEEE. Trans. Microwave Theory Tech.*, vol. MTT-23, pp. 588–591, July 1975.

[2] W. C. Chew and J. A. Kong, "Effects of fringing fields on the capacitance of circular microstrip disk," *IEEE. Trans. Microwave Theory Tech.*, vol. MTT-28, pp. 98–104, Feb. 1980.

[3] I. N. Sneddon, *Mixed Boundary Value Problems in Potential Theory*. New York: Wiley, 1966.

[4] Y. Nomura, "The electrostatic problem of two equal parallel circular plates," in *Proc. Phys. Math. Soc. Japan*, vol. 3, no. 23, 1941, pp. 168–180.

[5] Y. Nomura, "The forces on two parallel co-axial circular discs in uniform flow," *Sci. Rep. Tohoku Univ.*, vol. 29, pp. 304–318, 1940.

[6] G. N. Watson, *A Treatise on the Theory of Bessel Functions*. Cambridge University Press, 1922.

[7] S. Y. Poh, W. C. Chew, and J. A. Kong, "Approximate formulas for line capacitance and characteristic impedance of microstrip line, *IEEE. Trans. Microwave Theory Tech.*, vol. MTT-29, pp. 135–142, Feb. 1981.

The Measurement of the Electric Field Inside a Finite Dielectric Cylinder Illuminated by A Plane Wave

R. BANSAL, R. W. P. KING, AND T. T. WU

Abstract—**An experimental study of the distribution of the electric field induced inside a finite circular cylinder of water illuminated by an approximately plane electromagnetic wave is presented. The incident field was generated by using a monopole above the ground plane with a 90° corner reflector. The cylinder of water included a thin conducting tube at its center to shield the transmission lines leading to the probes. The graphs of selected measured distributions are displayed and interpreted. The measurements were carried out at 100, 300, and 600 MHz. The conductivity of the 50-cm long column of water was varied from approximately zero to 3.5 S/m. Both the amplitude and the phase of the induced electric field were measured in the experiment. Comparisons with a new theoretical solution developed by the authors are also included.**

I. INTRODUCTION

The interaction of electromagnetic radiation with a *finite* dielectric body is a problem of considerable practical interest. Such an investigation is of importance, for example, in the assessment of the biomedical hazards of EM radiation, the study of antennas attached to dielectric or poorly conducting aircraft, and the use of transponders embedded in biological organisms. The major focus of research in this area has been on the development of numerical solutions of EM-field problems involving three-dimensional bodies [1]–[5]. On the experimental side, thermal probes [6], [7] have been employed successfully to determine temperature

Manuscript received January 15, 1982; revised March 8, 1982. This work was supported in part by the Joint Services Electronics Program under Contract NOOO14-75-C-0648 with Harvard University.

R. Bansal was with the Gordon McKay Laboratory, Harvard University, Cambridge, MA 02138. He is now with the Department of Electrical Engineering and Computer Science, and the Institute of Materials Science of the University of Connecticut, Storrs, CT 06268.

R. W. P. King and T. T. Wu are with the Gordon McKay Laboratory, Harvard University, Cambridge, MA 02138.

0018-9480/82/0800-1282$00.75 ©1982 IEEE

distributions in simple models of mice and men. The temperature distribution can in turn be related to the square of the magnitude of the electric field; however, information about the polarization and phase of the electric field (required, for example, for a quantitative understanding of the operation and design of embedded transponders) cannot be extracted with thermal probing. Other investigators have used short dipole-type probes loaded with a microwave-detector-diode to measure the amplitude as well as the polarization of the induced electric field in thin slabs [8] and spheres [9] of simulated biological tissue. In this paper, we describe a systematic experimental study aimed at mapping the electric-field distribution inside a *finite* circular cylinder of water illuminated by a plane wave. A thin conducting tube was included at the center of the cylinder to shield the transmission lines leading to the probes. A significant feature of our study is the use of a vector voltmeter (HP 8405A) which allowed us to measure the phase of the electric field as well. The measured results are compared with a new theoretical solution [10], [11] developed by the authors.

II. Experimental Setup

A. Image Plane

The image plane used for our investigation was constructed from aluminum panels and measured 8 ft×24 ft. One of the panels contained a precisely machined circular hold of diameter 8.25 in with a groove along the periphery. This hole was used to accommodate the brass turntable on which the dielectric cylinder was mounted. Many other small holes equipped with plugs were also made in the image plane to allow a charge probe to pass through for the measurement of the incident electric field. Since the image plane used in our study was rather narrow at the lowest frequency of operation, improved isolation between the upper and lower half-spaces was achieved by supplementing the basic image plane from underneath by a chamber ("Faraday cage") made of aluminum screen.

B. Transmitting Antenna

The measurements were carried out at 100, 300, and 600 MHz, and at each of these frequencies a separate quarter-wave monopole was used for transmission. A 90° corner reflector, constructed by joining at right angles two 1/16-in thick aluminum plates of dimension 4 ft×6 ft, was erected behind the monopole at one end of the image plane. Each monopole was located (approximately) $\lambda/4$ from the corner. Besides increasing the signal level, use of the reflector also eliminated the reflections from the edge of the image plane where it was located.

The standard technique to protect the experimental setup from the influence of the incongruities in the room is to use suitable absorbers (of EM radiation) all around. However, the relatively low transmission frequencies made the use of absorbing material impractical. Therefore, the corner reflector was "extended" along both sides of the image plane by using aluminum screening carefully secured to wooden posts.

C. Cylinder

A hollow styrofoam tube filled with salt water was used to represent the upper half of the 'finite dielectric cylinder'; the lower half was, of course, automatically simulated by the image plane used in the experiment. The effective dielectric cylinder (referring to Fig. 1) had a total height $2h = 50$ cm and diameter $2b = 17.28$ cm. This styrofoam tube was mounted on the turntable by cutting a shallow circular groove in the bottom end of the tube and filling the groove with thermo-setting wax. The turntable was located at a distance of 18 ft from the corner reflector.

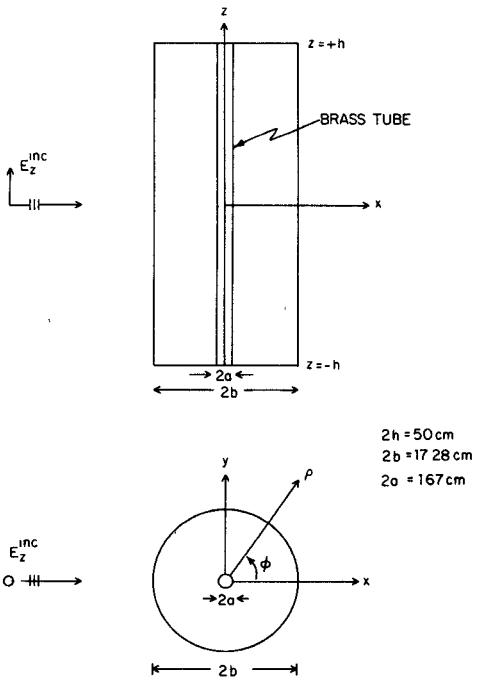

Fig. 1. Cylinder and coordinates.

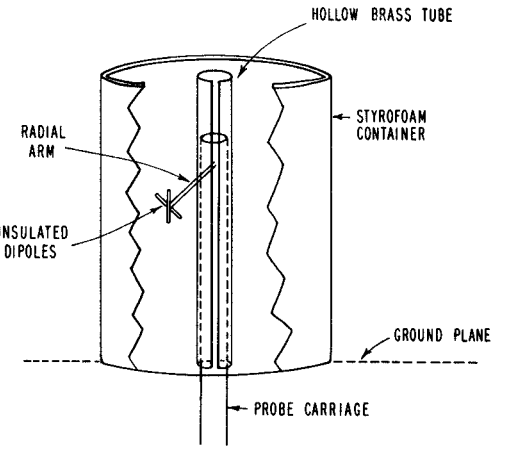

Fig. 2. Electric-field probes inside the cylinder (schematic).

D. Probes

In our experimental setup, the probes were supported by a radial arm (Fig. 2) and could, therefore, measure the magnitude and phase of E_z and E_ϕ without significant interference. The E_ρ component was not measured because of the perturbation caused by the radial arm. The probes were an orthogonal pair of insulated dipoles, designed as a precisely fabricated independent unit that could be readily connected and disconnected to the transmission lines through modified Microdot connectors. The probe ares were four 8.63-mm long pieces of 1.02-mm thick copper wire that were insulated by enclosing them in Alpha FIT-221-1/16-in shrinkable tubing ($\epsilon_r = 2.9$). The average wall thickness of the insulation (after thermal shrinking) was 0.25 mm. The total length of each dipole probe was 20 mm from tip to tip.

E. Probe Carriage

The ϕ-variation of the electric field was measured simply by rotating the turntable that supported the cylinder and the carriage assembly. The vertical location of the probes could be controlled by turning a rack-mounted knob located under the ground plane. The radial position of the probes could be changed in discrete steps only. The transmission lines and the associated probe carriage were shielded by a concentric vertical brass tube, 25 cm long and 16.7 mm in diameter, soldered to the base of the turntable. A 6.4-mm longitudinal slot was cut along the entire length of this tube to accommodate the vertical movement of the radial arm carrying the probes (Fig. 2).

F. Detector Circuit

The EM signals picked up by the dipole probes were carried by Microdot transmission lines and were fed to a vector voltmeter (HP 8405A) through a manually operated multiport coaxial switch. One of the channels of the vector voltmeter was hooked to a phase reference signal derived from the transmission system.

III. Measurements

A. Incident Wave

The incident electric field (E_z^{inc}) at the image plane (with the dielectric cylinder removed) was measured by means of a charge probe, a bare monopole 1.7 mm in diameter and 5.1 cm in height. Two kinds of measurements were made at each of the three frequencies. One set was comprised of measurements made parallel to the direction of propagation and tested the traveling-wave nature of the incident field. The second set consisted of measurements made perpendicular to the direction of propagation with a view to ascertaining the nature of the wavefront. The results [10] indicated that less than 20 percent of the incident power was reflected from the far edge of the image plane at any transmission frequency. Also, it was found that at both 100 MHz and 300 MHz, the wavefront was very nearly plane; however, at 600 MHz, reflections from the aluminum screen on the sides resulted in small ripples in the magnitude and phase of E_z^{inc} transverse to the direction of propagation.

B. Constitutive Parameters of Solutions

At a given frequency and temperature, the electrical properties of a salt-water solution can be fully characterized by a real permittivity $\epsilon = \epsilon_0 \epsilon_r$ and a real effective conductivity σ. (The permeability of all the solutions used in the experiment was assumed to be that of free space.) Since the constitutive parameters of salt water vary considerably with frequency in the experimental range of 100–600 MHz, separate measurements were carried out at each of the frequencies of interest. These measurements made use of an experimental apparatus previously designed and described by Smith [12], [13].

C. Electric Field in the Cylinder

The distributions of E_z and E_ϕ were obtained over the range (with reference to Fig. 1) $-\pi \leq \phi \leq 0, 0 \leq z \leq h$. (The actual experimental data points spanned the narrower range 4 cm $\leq z \leq$ 20 cm ($h = 25$ cm), partly due to the mechanical limitations in the system and partly because calibration errors may be introduced in the response of a probe if it approaches too close to an interface [14].) The distributions of E_z and E_ϕ for $0 \leq \phi \leq \pi$, as well as for $-h \leq z \leq 0$, can be readily deduced from the measured distributions by using the symmetry properties listed in Table I for an incident electric field polarized parallel to the axis of the cylinder.

TABLE I
SYMMETRY OF $\vec{E}$

	E_ρ	E_ϕ	E_z
z	odd	odd	even
ϕ	even	odd	even

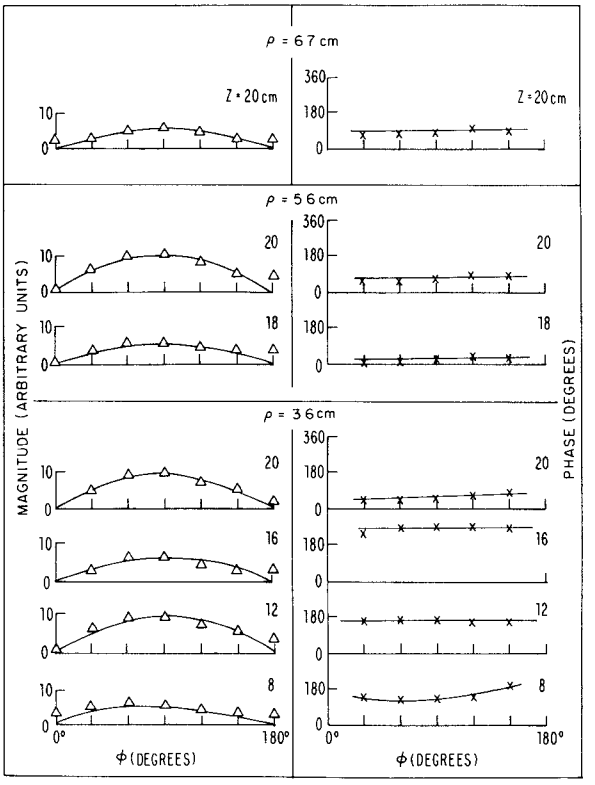

Fig. 3 Measured distribution of transverse electric field E_ϕ; $f = 300$ MHz, $\sigma = 0.27$ S/m.

The conductivity of the solutions was varied during the course of the experiment from approximately zero (distilled water) to 3.5 S/m. Complete sets of experimental data are available in [10] in both graphical and tabular form. Typical distributions of E_z and E_ϕ are shown in Figs. 3 and 4. (The solid lines in these figures are smooth curves drawn through the measured points in accordance with the symmetry properties of Table I.) Significant features of the measured distributions are discussed below.

1) E_ϕ has a relatively simple distribution in all the cases. As shown in Fig. 3, $|E_\phi|$ vanishes at $\phi = 0°$ and $\phi = 180°$ and smoothly reaches a maximum near $\phi = \pm 90°$ for all values of ρ and z. Also, at 100 and 300 MHz, $|E_\phi|$ is quite small compared to $|E_z|$ except near the ends of the cylinder. It should be noted that an incident plane wave with a z-polarized electric field induces *only* the E_z component in an infinitely long dielectric cylinder. When the cylinder is truncated at $z = \pm h$, E_z generally remains the dominant component throughout the cylinder, but near the ends ($z = \pm h$) E_ϕ and E_ρ (see Section IV) also become significant.

2) At 600 MHz, the circumference of the dielectric cylinder is approximately equal to the free-space wavelength ($k_0 b = 1.09$) and a kind of "transverse resonance effect" [15] becomes ap-

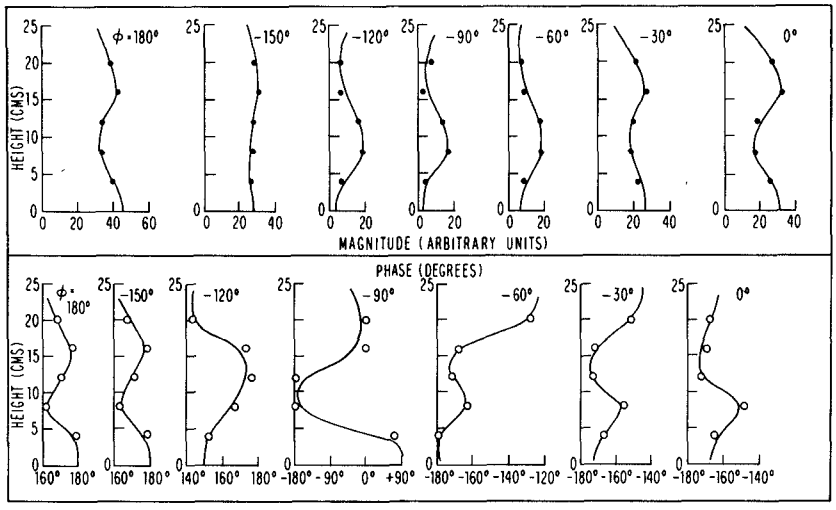

Fig. 4. Measured distribution of axial electric field E_z; $f = 300$ MHz, $\sigma \simeq 0$ S/m, $\rho = 6.4$ cm.

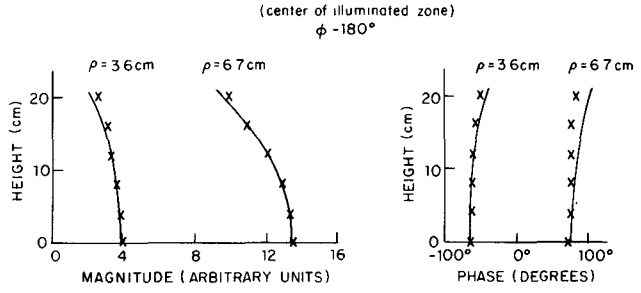

Fig 5. Distribution of axial electric field E_z; $f = 300$ MHz, $\epsilon_r = 78$, $\sigma = 3.2$ S/m. —Experiment. $\times\times\times$ Theory (zeroth iteration).

parent in the distribution of E_ϕ. Unlike at the lower frequencies, a fairly substantial transverse component of the electric field is induced *throughout* the dielectric cylinder except in the immediate vicinity of $z = 0$ where symmetry conditions force E_ϕ to go to zero.

3) The effect of increasing the conductivity of the solution was twofold. First, with an increase in the conductivity, the magnitudes of E_z and E_ϕ decrease throughout the cylinder because of the increased absorption by salt water. More significantly, an increase in the conductivity of the solution also damps out the "higher mode content" in the axial distribution of E_z (Figs. 4 and 5).

IV. Comparison with Theory

An approximate hybrid iterative solution suitable for finite cylinders with large ϵ_r has been recently developed by the authors [10], [11]. It combines the analytical eigenfunction expansion method (internal absorption problem) with a single surface integral equation (external scattering problem). Since the internal problem is solved analytically, the theoretical solution can handle the homogeneous dielectric cylinder and the cylinder with a concentric metal tube (Fig. 1) with equal ease. A sample of the comparison between the measured distributions and the theoretically computed results is presented in Fig. 5. The agreement is seen to be fairly good. Also, it was found [10] from the theoretical solution that when the salt water in the cylinder has a moderately high loss tangent, the resulting large attenuation makes the thin metal tube at the center nearly "invisible" to the incident field, and the distributions of electric field in the experimental cylinder are, therefore, good approximations of the distributions in the corresponding *homogeneous* cylinders of salt water, except at points very close to the axis. It will be recalled from Section II-*D* that E_ρ was not measured in the experiment because of the interference from the radial arm supporting the probes. It was found from our theoretical solution that $|E_\rho|$ is generally negligible compared to $|E_z|$ over most of the length of the cylinder except near the ends.

V. Summary

A detailed experimental study has been made of the electric-field distributions inside a finite circular cylinder of salt water when illuminated by a plane wave whose electric vector is polarized parallel to the axis of the cylinder. The measurement techniques have been described and significant features of the measured data have been discussed. Comparisons with a new theoretical solution have also been presented.

Acknowledgment

The authors wish to thank the members of the review board for their helpful comments and suggestions.

References

[1] D. E. Livesay and K.-M. Chen, "Electromagnetic fields induced inside arbitrarily shaped biological bodies," *IEEE Trans. Microwave Theory Tech.*, vol. MTT-22, pp. 1273–1280, Dec. 1974.

[2] P. W. Barber, "Resonance electromagnetic absorption by nonspherical dielectric objects," *IEEE Trans. Microwave Theory Tech.*, vol. MTT-25, pp. 373–381, May 1977.

[3] T.-K. Wu, "Electromagnetic fields and power deposition in body-of-revolution models of man," *IEEE Trans. Microwave Theory Tech.*, vol. MTT-27, pp. 279–283, Mar. 1979.

[4] M. A. Morgan and K. K. Mei, "Finite-element computation of scattering by inhomogeneous penetrable bodies of revolution," *IEEE Trans. Antennas Propagat.*, vol. AP-27, pp. 202–214, Mar. 1979.

[5] C. H. Durney, "Electromagnetic dosimetry for models of humans and animals: A review of theoretical and numerical techniques," *Proc IEEE*, vol. 68, pp. 33–40, Jan. 1980.

[6] A. W. Guy, "Analyses of electromagnetic fields induced in biological tissues by thermographic studies on equivalent phantom models," *IEEE Trans. Microwave Theory Tech.*, vol. MTT-19, pp. 205–214, Feb. 1971.

[7] O. P. Gandhi, "Conditions of strongest electromagnetic power deposition in man and animals," *IEEE Trans. Microwave Theory Tech.*, vol. MTT-23, pp. 1021–1029, Dec. 1975.

[8] B. S. Guru and K.-M. Chen, "Experimental and theoretical studies on electromagnetic fields induced inside finite biological bodies," *IEEE Trans. Microwave Theory Tech.*, vol. MTT-24, pp. 433–440, July 1976.

[9] H. Bassen, P Herchenroeder, A. Cheung, and S. Neuder, "Evaluation of an implantable electric field probe within finite, simulated tissues," *Radio Sci.*, vol. 12, pp. 15–25, Nov.–Dec. 1977.

[10] R. Bansal, "A theoretical and experimental study of electromagnetic fields in finite dielectric cylinders," Ph.D. thesis, Div. Appl. Sciences, Harvard Univ., Cambridge, MA, 1981.

[11] R. Bansal, T T Wu, and R W P. King, "Analysis of finite dielectric bodies in a plane-wave field," *Instit. Elect. Eng. Proc.*, accepted for publication.
[12] G. S. Smith, "A theoretical and experimental study of the insulated loop antenna in a dissipative medium," Div. Eng. Appl. Phys., Harvard Univ., Cambridge, MA, Tech. Rep. No. 637. Apr. 1973.
[13] R. W. P. King and G. S. Smith, *Antennas in Matter*. Cambridge, MA: The M.I.T. Press, 1981, pp. 767–770.
[14] G. S. Smith, "The electric-field probe near a material interface with application to the probing of fields in biological bodies," *IEEE Trans. Microwave Theory Tech.*, vol. MTT-27, pp. 270–278, Mar. 1979.
[15] R. W. P. King, B. Sandler, T. T. Wu, R. W Burton, C. C. Kao, and L. C. Shen, "Surface currents and charges on an electrically thick conducting tube in an *E*-polarized, normally incident, plane-wave field, 1, theory," *Radio Sci.*, vol. 11, pp. 687–699, Aug.–Sept. 1976.

Automatic Noise Temperature Measurement Through Frequency Variation

VICTOR D. LAROCK, MEMBER, IEEE, AND RENE P. MEYS, MEMBER, IEEE

Abstract — **The dependence of two-port noise temperature on the source reflection factor does not lend itself to easy automated measurement. This paper shows that a noise analysis performed over a small frequency interval centered about the frequency of interest and with a source circuit having fast phase variations leads to a straightforward solution of the problem. The conditions for applying the procedure are broad enough to enable measuring most components like transistors and amplifiers over the entire microwave range. An example of practical implementation is presented.**

I. Introduction

The determination of the dependence of the noise temperature on the source reflection factor requires measurements with various source impedances. These are obtained manually by means of stubs, line stretchers, and the like.

Such devices are cumbersome to operate automatically, although a mechanical tuner driven by stepper motors has been proposed [1]. Another approach uses varactor-controlled tuners [2]. Due to the small capacitance variations that can be achieved through microwave varactors, this kind of tuner operates only over a limited frequency range.

Moreover, both tuners exhibit unpredictable losses, which have to be taken into account for accurate noise measurements. Accordingly, they must be determined for every setting at every frequency.

Thus, the challenge was: could one imagine a set of electrically controlled impedances or reflection factors sufficient to determine the noise temperature and meeting the extra constraint of easily accountable losses?

II. An Automated Procedure for Determining the Noise Temperature

A guide to this choice is [3], where it is shown that the dependence of the noise temperature T_n on the source reflection factor $S = |S| \cdot e^{j\varphi_s}$ can be expressed as

$$T_n = \frac{T_a + |S|^2 T_b + 2T_c |S| \cos(\varphi_s + \varphi_c)}{1 - |S|^2}. \quad (1)$$

Manuscript received November 11, 1981; revised March 3, 1982.
The authors are with the Laboratoire de Radioélectricité Université, Libre de Bruxelles, Brussels, Belgium.

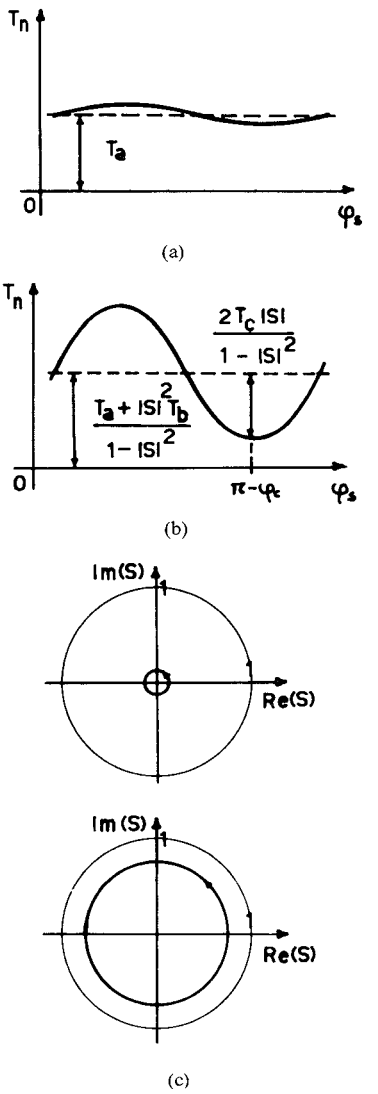

Fig. 1. The theoretical dependence of the noise temperature on the source reflection factor with (a) small $|S|$ and (b) significant $|S|$. (c) Shows the corresponding S-loci

The parameters T_a, T_b, T_c, and φ_c are related to the noise waves model for the two-port, (see [3] and [4]), and are determined experimentally in two steps.

a) *Measurements with a matched source*: With an ideal source ($S = 0$) the noise temperature would be T_a. For any real source having small mismatch $|S|$, (1) becomes

$$T_n \simeq T_a + 2T_c |S| \cos(\varphi_s + \varphi_c). \quad (2)$$

This relation is plotted as a function of φ_s in Fig. 1(a); it yields T_a as the mean value of $T_n(\varphi_s)$.

b) *Measurements with a significant source reflection factor*: The general case (1) is plotted in Fig. 1(b), where it can be seen that: the mean value of the curve gives T_b if $|S|$ and T_a are known; the amplitude of the sine wave is related to T_c; and the position of the curve defines φ_c. The S variations involved appear in Fig. 1(c). They were formerly achieved by a line stretcher inserted between the source and the DUT.

Now, automation clearly requires moving on the reflection factor loci electrically. To this end, use is made of two factors. a) Phase variations can be obtained at the output of a long section of line by slightly changing the frequency of analysis, say by 1

0018-9480/82/0800-1286$00.75 ©1982 IEEE